J. Fluid Mech. (2004), *vol.* 510, *pp.* 145–168.
DOI: 10.1017/S002211200400936X Printed in the United Kingdom

On the glug-glug of ideal bottles

By CHRISTOPHE CLANET AND GEOFFREY SEARBY

Institut de Recherche sur les Phénomènes Hors Equilibre,
UMR 6594, 49 rue F. Joliot Curie, BP 146, 13384 Marseille, France

(Received 15 July 2003 and in revised form 22 February 2004)

We present an experimental study of the emptying of an ideal vertical bottle under gravity g. The idealization reduces the bottle to a cylinder of diameter D_0, length L, closed at the top and open at the bottom through a circular thin-walled hole of diameter d, on the axis of the cylinder. The study is performed in the low-viscosity limit. The oscillatory emptying of the 'bottle' is referred to as the glug-glug, and is characterized by its period T, whereas the whole emptying process is characterized by a time T_e. Concerning the long time scale T_e, we show that:

$$\frac{T_e}{T_{e0}} = \left(\frac{D_0}{d}\right)^{5/2},$$

where $T_{e0} \approx 3.0L/\sqrt{gD_0}$ is the emptying time of an unrestricted cylinder. On the short time scale T, we show that the physical origin of the oscillations lies in the compressibility of the surrounding gas. The period can be written as:

$$T = \frac{L}{\sqrt{\gamma P_0/\rho}}\Phi(\bar{z}_i/L),$$

where γ is the ratio of specific heats of the gas, P_0 its pressure and ρ stands for the density of the liquid. The function Φ is dimensionless and changes with the relative position of the liquid interface $\bar{z}_i/L$. Finally, this analysis of time scales involved in the emptying of vertical cylinders is applied to other liquid–gas oscillators.

1. Introduction

An image of life is a return to the thermodynamic equilibrium of death via the oscillations of our heartbeats. For the particular case of humans, the ratio of the long time scale of life to the short time scale of the heart beat is of the order of 2×10^9.† All living creatures follow the same rule with different ratios, and so do the following *Clepsydrae*. The common experience of the emptying of a vertical bottle initially full of liquid, surrounded by air, and submitted to the acceleration due to gravity g, reveals that the liquid flows out of the bottle through an alternating succession of jets of liquid and admissions of air bubbles. This oscillatory path back to the equilibrium is referred to by the onomatopoeic glug-glug and is characterized by the period of the oscillations T. This oscillatory behaviour starts at the opening and continues until the bottle is empty, that is all along the emptying time, or lifetime T_e. An example of such behaviour is presented in figure 1. Figure 1(*a*) shows the geometrical characteristics of the bottle and figures 1(*b*) and 1(*c*) show the evolution of the apparent weight of the

† According to Calder (1984), the ratio (life span)/(cardiac cycle) for mammals of mass M is of the order of $2.5 \times 10^9\, M^{-0.05}$. For birds, this ratio scales as $2.32 \times 10^9\, M^{-0.04}$.

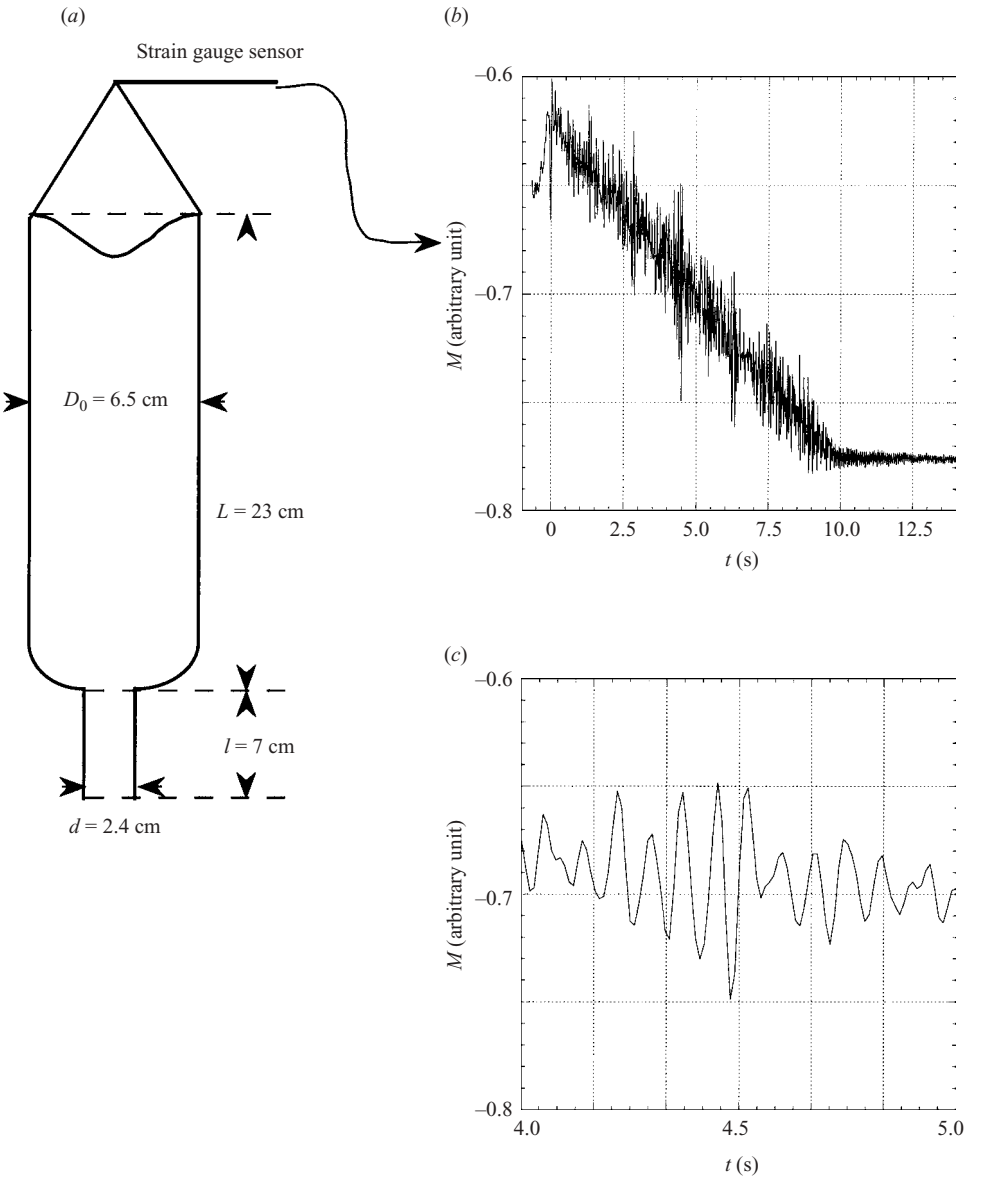

FIGURE 1. Example of bottle emptying obtained with ethanol: (*a*) geometrical characteristics of the bottle; (*b*) general evolution of the dynamic weight; (*c*) detailed evolution of the weight.

bottle, obtained during the emptying using a strain gauge sensor. We first observe in figure 1(*b*), that the order of magnitude of the emptying time is $T_e \approx 10$ s. Despite the oscillations, we also observe in this figure that the suspended mass decreases almost linearly in time. Figure 1(*c*) provides a close view of the evolution of the signal in the time zone $t \in [4\,\text{s}, 5\,\text{s}]$. This zoom, reveals that the apparent weight oscillates with a characteristic frequency $1/T \approx 14$ Hz that is $T \approx 0.07$ s. The life of this bottle can thus be characterized by the ratio $T_e/T \approx 140$.

To understand the physical laws governing the existence of this system, we first reduce the problem to the emptying of a vertical cylinder of diameter D_0 and length

L, closed at the top and open at the bottom through a circular thin-walled hole of diameter d, on the axis of the cylinder. The cylinder being initially filled with a liquid of density ρ, viscosity ν and surface tension with the surrounding air σ. At $t=0$ we open the hole d and look for the laws governing both T_e and T as a function of the interface location z_i (see figure 3). The problem can formally be written:

$$T_e = \mathscr{F}(GP, PC), \quad T = \mathscr{G}(GP, PC), \tag{1.1}$$

where GP stand for the geometrical properties ($GP=\{L, D_0, d, z_i\}$) and PC for the physical characteristics ($PC=\{g, \rho, \nu, \sigma, \beta\}$), were $\beta \equiv 1/\rho\,(\partial\rho/\partial P)_s$ is the compressibility of the surrounding gas at constant entropy. To define the precise domain of our investigation embedded in this huge parameter space, several preliminary remarks are required.

Since the pioneering work of Dumitrescu (1943), cited by Prandtl (1952), much work has been devoted to the singular limit $d=D_0$, where a long bubble of diameter D_0 is observed rising with the constant velocity $U_b \approx 0.33\sqrt{gD_0}$. In this limit, no oscillations are observed and the emptying time is straightforward: $T_{e0} \approx 3.0L/\sqrt{gD_0}$. For holes of diameters smaller than but of the order of D_0, we first observe such a large bubble rising to the top prior to the onset of the oscillations. For diameters $d \lesssim D_0/2$, the oscillations start from the opening.

Among the different studies devoted to the limit $d=D_0$, the careful experimental work of Zukoski (1966) shows that the above velocity U_b holds, provided viscous and surface-tension effects can be neglected. More precisely, Zukoski finds that viscosity alters U_b if the Reynolds number $Re \equiv U_b D_0/\nu$ is smaller than 100. Using the expression $U_b \approx 0.33\sqrt{gD_0}$, the above limit can be expressed as a function of the length ratio $D_0/l_\nu > 45$, where $l_\nu \equiv (\nu^2/g)^{1/3}$ is the viscous length. In the case of water, $l_\nu \approx 46\,\mu\text{m}$ and the non-viscous regime is obtained for $D_0 > 2\,\text{mm}$.

Concerning the effect of surface tension, Zukoski shows experimentally that this effect is negligible if the diameter of the tube is larger than $D_0 \geqslant 4.5a$, where a is the capillary length of the liquid, defined as $a \equiv \sqrt{2\sigma/(\rho g)}$. If the diameter of the tube becomes smaller than this limit, the velocity of the bubble decreases until the point $D_0 \approx 1.9a$, where the flow of the liquid out of the tube is prevented by capillary effects. In the case of water, $a \approx 3.8\,\text{mm}$, and the critical diameter under which the emptying time tends to infinity is $D_{0c} \approx 7.2\,\text{mm}$.

Our study is conducted in the non-viscous limit $45\,l_\nu < 1.9\,a$, that is, with liquids characterized by a Kapitsa number $Ka = (\rho^3 g \nu^4/\sigma^3)^{1/6} < 0.06$. Using these fluids, the diameter ratio d/D_0 is kept in the domain $[D_{0c}, D_0]$. The domain of our investigation H, is summarized in figure 2 in the plane of $(d/D_0, Ka)$.

Because of industrial applications, several studies have already been devoted to bottle emptying, a review of which can be found in Dukler & Fabre (1994) and Fabre & Line (1992). Most of these studies relate the rising velocity of the gas phase U_b to the opening diameter d through a relation of the form $U_b = C\sqrt{gd}$, and investigate the behaviour of the coefficient C with the geometry of the neck, the ratio of the gas to liquid density, and the nature of the liquid. Concerning the short time scale, even if sandclock intermittencies have been studied in granular science (Bideau, Madani & Hansen 1994; Le Pennee *et al.* 1994), to our knowledge, the characteristics of the oscillations in 'liquid-clocks' such as the glug-glug have never been studied.

In § 2, we present the experimental set-up. The results obtained are discussed in § 3, and modelled in § 4. The ideas developed are applied to other pulsating clepsydrae in § 5 conclusions are given in § 6.

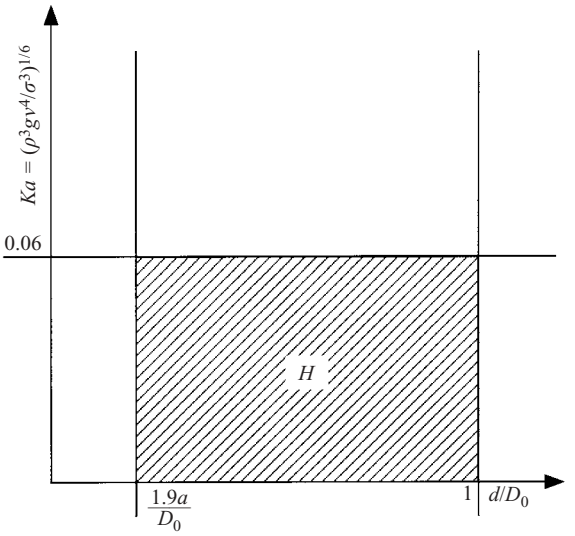

FIGURE 2. Investigation domain.

2. Experimental set-up

The experimental set-up used to measure the long time of emptying, T_e, and the short time of the oscillation, T, is presented in figure 3(a). The Newtonian liquid is initially contained in the tank whose pressure is kept equal to the atmospheric pressure through large openings. The door being initially closed, we open the valves 1 and 2 and fill the tube using a pump. Once the tube is filled, the pump is stopped, the two valves are closed, and the lower door is opened quickly at $t = 0$.

As the liquid starts to flow out of the tube, the CCD camera records the trajectory of the upper interface, while the pressure sensor shows the pressure fluctuations in the upper gas volume. In other words, the CCD camera provides information on the long time scale while the pressure sensor focuses on the short time scale. Both devices are synchronized by the TTL pulse that triggers simultaneously the laser beam seen by the camera and the acquisition of the pressure signal.

The experimental way to approach the functions $\mathscr{F}$ and $\mathscr{G}$ presented in § 1 is to vary the variables (GP, PC) independently over as large a range as possible. The geometrical properties $GP = \{L, D_0, d, z_i\}$, were changed using holes of different diameters and three tubes. All the reported experiments were conducted using a thin-walled hole with an edge angle, $\alpha = 20°$ (figure 3c). The diameters, d, are members of the family $d(\text{mm}) \in [174, 132.9, 101.5, 77.5, 59.2, 45.2, 34.5, 26.4, 20.1, 15.35, 12.4, 11.7, 10, 9]$. The 'quasi' power-law evolution of the diameters simplifies the identification of an eventual power law dependency on d. Concerning the variation of the length L, and of the diameter D_0, we have used three different cylinders whose properties are summarized in table 1. This tube selection enables an independent variation of the diameter (tubes 1 and 3) and of the length (tubes 2 and 3), the aspect ratio being the same for tubes 1 and 2 and being multiplied by two between tubes 1 and 3. The physical characteristics $PC = \{\rho, \nu, \sigma, g, \beta\}$, were changed using liquids of different properties: water, ethanol and a mixture water + glycerol. Their properties are summarized in table 2, where the last two columns present the capillary length and the Kapitsa number. The parameters g and β are constant in all the experiments, $g = 9.81\,\text{m}\,\text{s}^{-2}$ and $\beta = 1/(\gamma P_0)$, where $\gamma = 1.4$ for air and P_0 is the ambient pressure.

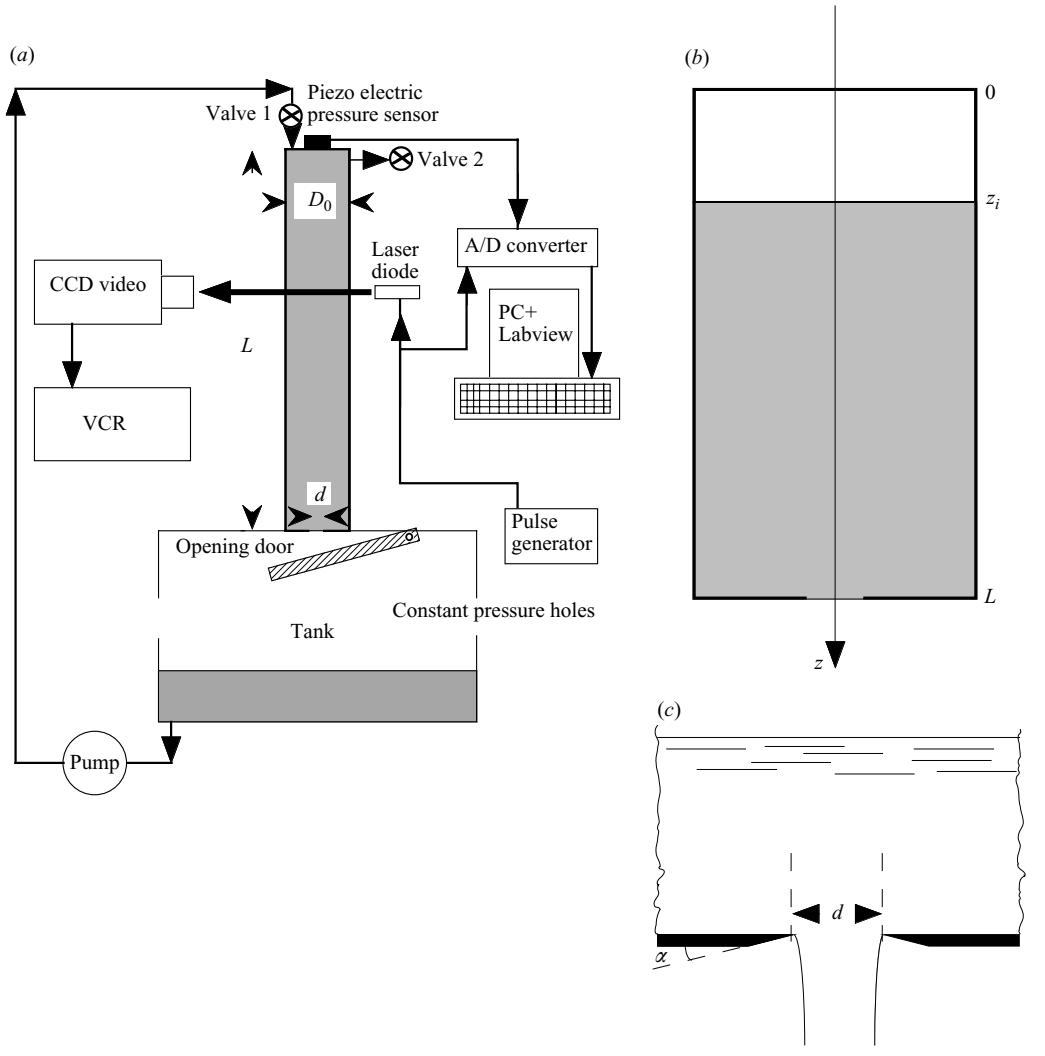

FIGURE 3. Experimental set-up: (*a*) general principle of the apparatus, (*b*) schema and orientation of axes, (*c*) close-up view of the hole.

Tube	L (m)	D_0 (m)	L/D_0
1	1.75	0.174	10.05
2	0.865	0.0789	10.96
3	1.75	0.0789	22.18

TABLE 1. Geometrical characteristics of the tubes.

Fluid	ρ(kg m^{-3})	ν (m^2 s^{-1})	σ (kg s^{-2})	a (m)	Ka
Water	1000	10^{-6}	0.073	3.8×10^{-3}	0.017
Ethanol	810	1.5×10^{-6}	0.025	2.5×10^{-3}	0.034
Water + glycerol	1050	3.5×10^{-6}	0.070	3.7×10^{-3}	0.057

TABLE 2. Physical properties of water, ethanol and water + glycerol at 22 °C.

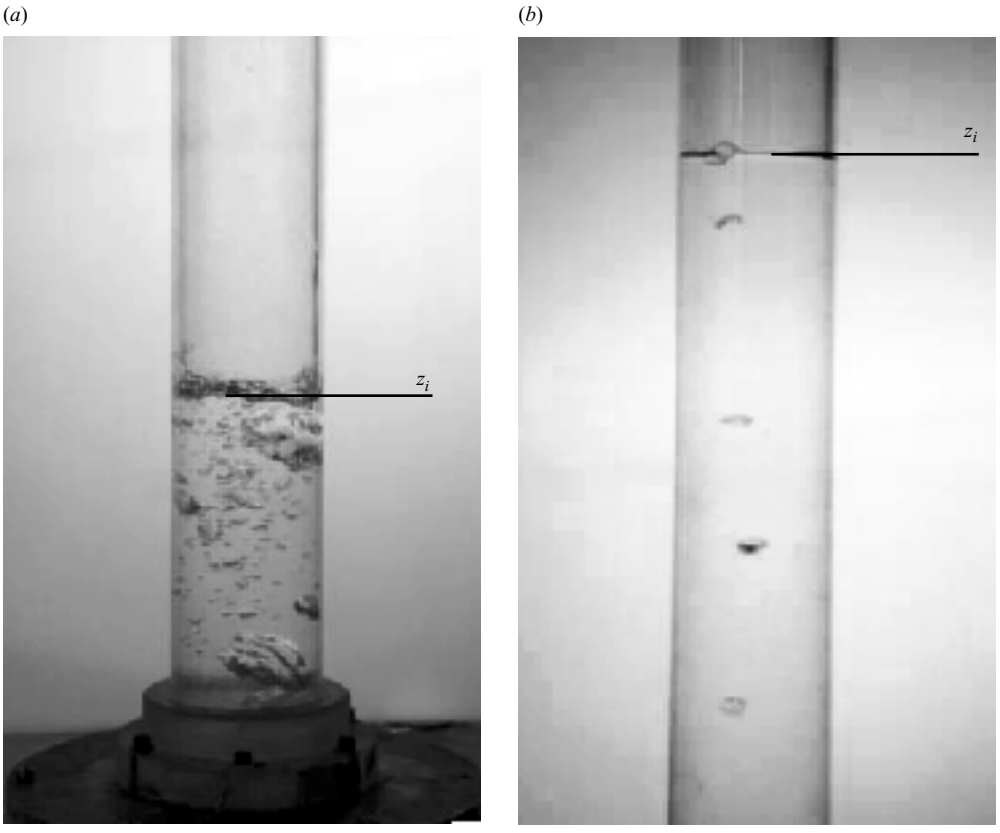

FIGURE 4. Examples of pictures treated to extract the interface location z_i: (*a*) tube 2 with water and $d = 34.5\,\text{mm}$; (*b*) tube 2 with water and $d = 10\,\text{mm}$.

3. Experimental results

3.1. *On the long time scale T_e*

Two representative examples of images treated to extract the interface location, z_i, are presented in figure 4. For all hole diameters, the upper interface is well defined and the experimental error associated with this measurement is small ($\leqslant 1\%$).

Using the notation and axis orientations presented in figure 3(*b*), we first present the experimental results obtained on the long time scale, T_e. Using tube 1 with water, the typical time evolution of the upper interface is presented in figure 5(*a*), with the initial condition, $z_i(t=0)=0$. Despite some acceleration towards the end of the process, it can be seen that the interface is characterized by a quasi-constant speed over most of the emptying. This velocity decreases as the diameter of the hole, d, decreases. Typically, the velocity is of the order of $0.3\,\text{mm}\,\text{s}^{-1}$ for $d = 10\,\text{mm}$ and increases up to $53.5\,\text{mm}\,\text{s}^{-1}$ for $d = 77.5\,\text{mm}$. These trajectories can be compared to those of figure 5(*b*), obtained in Torricelli's regime with the same tube and the same hole diameters but with an open top instead of a closed one. In Torricelli's regime, we observe a decelerated trajectory. Apart from the shape of the trajectory, the comparison between the glug-glug and Torricelli's regimes reveals that the emptying time T_e is always one order of magnitude larger in the glug-glug regime.

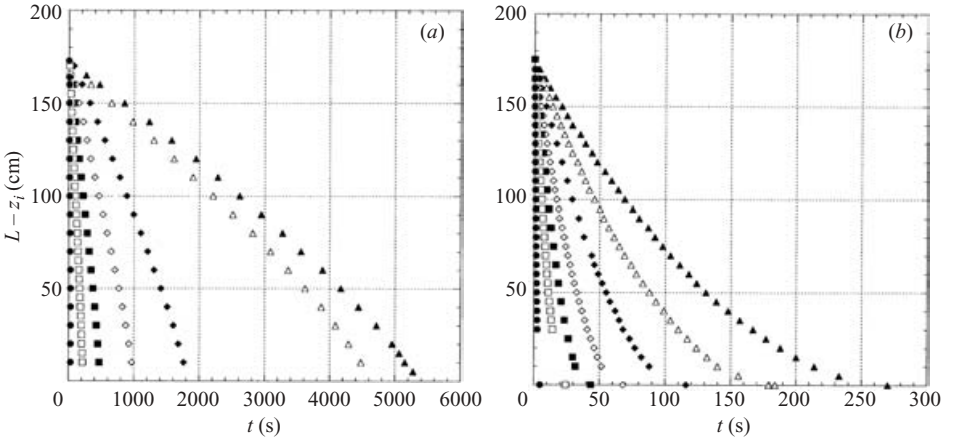

FIGURE 5. Tube 1 and water: trajectory of the upper interface during the emptying, for two different limit conditions: (*a*) top closed – glug-glug regime; (*b*) top opened – Torricelli's regime, and different hole diameters: ▲, $d = 10$ mm; △, 12.4 mm; ◆, 15.35 mm; ◇, 20.1 mm; ■, 26.4 mm; □, 34.5 mm; ●, 77.5 mm.

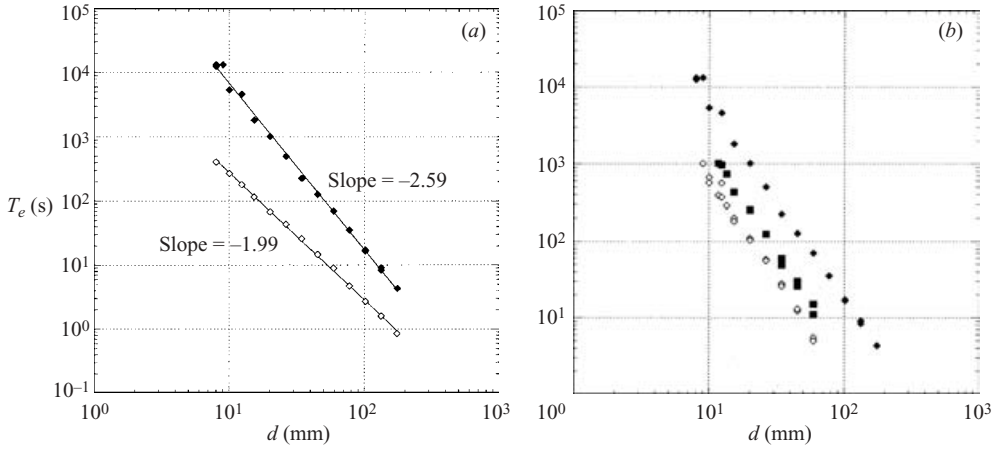

FIGURE 6. (*a*) Tube 1 and water: emptying time T_e as a function of the hole diameter d mm, ◆, glug-glug regime; ◇, Torricelli's regime. (*b*) glug-glug regime with water: ◆, tube 1; ◇, tube 2; ■, tube 3.

Figure 6(*a*) presents the emptying time, T_e, as a function of the diameter of the hole, d, for tube 1 and water in the two previous regimes. The striking feature is the power law dependency on d in both regimes: $T_e \propto d^{\alpha}$, where $\alpha \approx -2.59$ in the glug-glug regime and $\alpha \approx -1.99$ in Torricelli's regime. This latter result is expected from the well-known expression for the interface velocity $v(z_i) = C(d/D_0)(d/D_0)^2\sqrt{gz_i}$. The function $C(d/D_0)$ together with the asymptotic character of $v(z_i)$ has been studied in Clanet (2000).

It must be emphasized that the diameter of the hole d varies in this figure from the blocking limit $d = D_{0c} \approx 8$ (mm) for water to the tube diameter $d = D_0$. The power law $T_e(d)$ extends over this whole domain, thus suggesting that on the long time scale T_e, the singular limit $d = D_0$ can be considered as governed by the same physics as smaller diameters.

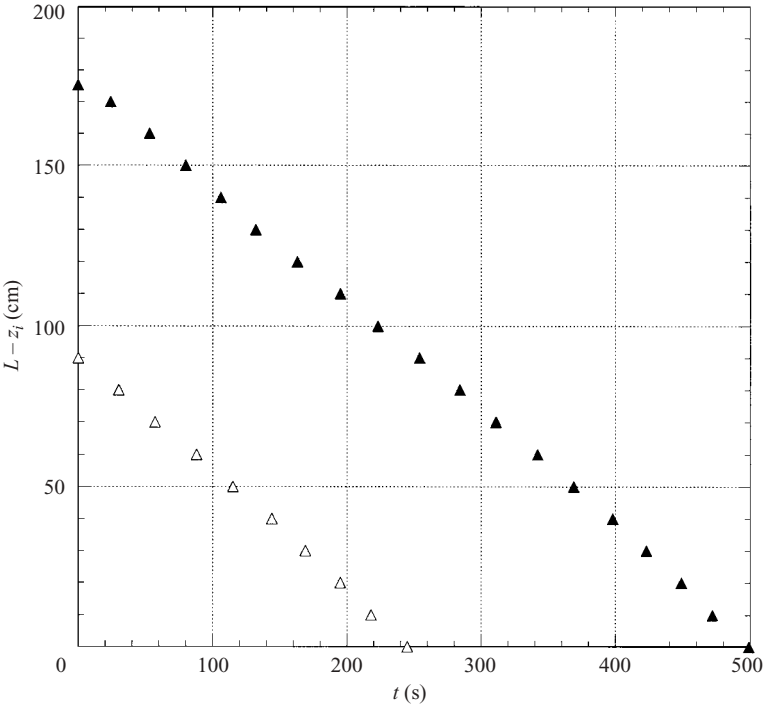

FIGURE 7. Trajectory of the interface $z_i(t)$ for two different initial conditions: ▲, $z_i(t=0)=0$ cm; △, $z_i(t=0)=85$ cm.

The influence of the geometry (L, D_0) on the emptying time T_e in the glug-glug regime is presented in figure 6(*b*) for the three different tubes 1, 2 and 3. From this figure, we conclude that the geometry does not change the power law, but alters the absolute value of T_e, the life time being longer for a cylinder of greater volume.

The effect of the initial location of the interface $z_i(t=0)$ on its dynamics is presented in figure 7, where the trajectories obtained, in tube 1 and water, with $z_i(t=0)=0$ cm and $z_i(t=0)=85$ cm are reported. This figure shows that neither the linear character of the trajectory nor the slope of this line is affected by the difference in the initial condition. There is no memory effect in the physics of the long time scale T_e.

Concerning the liquid properties, we present in figure 8, the evolution of the emptying time T_e as a function of the diameter of the hole d, measured in tube 1 with the three different liquids presented in § 2. We observe in this figure that the emptying time is not sensitive to a change in density, surface tension or viscosity. This statement holds provided that the diameter of the hole is larger than the capillary length, and that the Kapitsa number is smaller than unity.

3.2. *On the short time scale T*

For the short time scale T, the law $T=\mathscr{G}(GP, PC)$ is investigated using the unsteady pressure signal delivered by the piezo-electric sensor located in the gas phase (see figure 3). A typical signal obtained with tube 2 and water with a 10 mm hole diameter is presented in figure 9(*a*) for the initial condition $z_i(0)=0$ cm. At $t=0$, the hole is opened and the oscillations start and continue until $t=T_e\approx 570$ s. The detail of the oscillations is presented at different equally spaced times in figures 9(*b–e*).

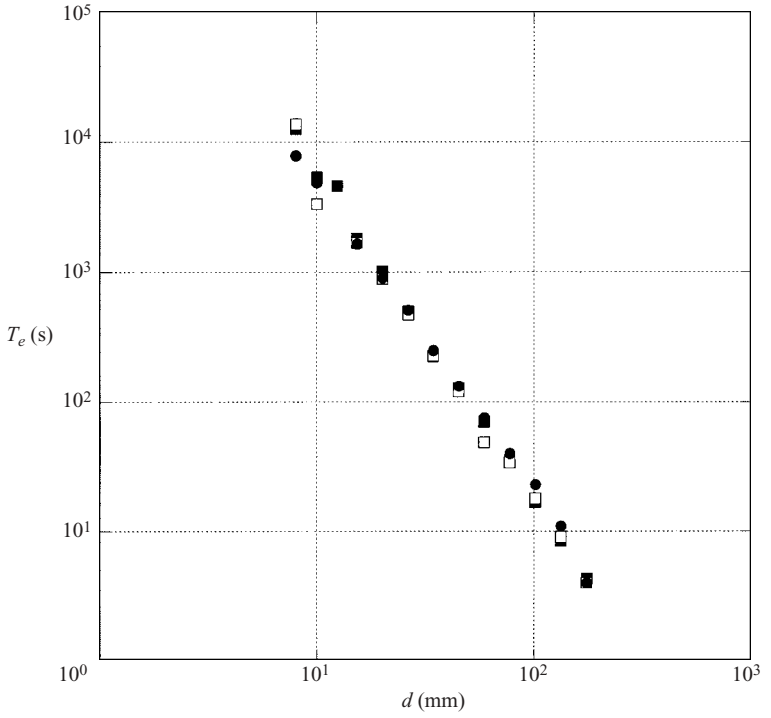

FIGURE 8. Evolution of the emptying time T_e with the diameter of the hole d for different liquids: ■, deionised water; □, water + glycerol; ●, ethanol.

First, considering the waveform presented in the different zones, we observe that the oscillations are almost sinusoidal at the beginning with a clear left–right and up–down symmetry. As the interface moves down, the oscillations become nonlinear and figure 9(*e*) clearly shows that left–right symmetries have been lost. According to these figures, the nonlinear character of the oscillations increases as the interface moves closer to the hole. This general feature was observed in all experiments.

Each of the zooms presented in figure 9, reveals that locally, a mean period of oscillation T can be defined and that period changes on the long time scale. More precisely in this example, the period of oscillation increases with time from $T(7.5\,\mathrm{s}) \approx 0.2\,\mathrm{s}$ to $T(557.5\,\mathrm{s}) \approx 0.38\,\mathrm{s}$ with the intermediate values $T(202.5\,\mathrm{s}) \approx 0.29\,\mathrm{s}$ and $T(407.5\,\mathrm{s}) \approx 0.32\,\mathrm{s}$.

The evolution of the period of oscillation T, measured in tube 2 with water and with different holes diameters, is presented in figure 10 as a function of the interface location z_i/L. We first observe in figure 10 that the period of oscillation T is a function of both the interface location and of the diameter of the hole. The smaller the diameter d, the larger the period T. We also notice that for diameters larger than 15 mm, the period increases from $z_i/L = 0$ to $z_i/L \approx 0.5$ and then decreases until $z_i/L \approx 1$. We also observe that the evolution of the period obtained with $d = 26.4\,\mathrm{mm}$ is identical to that measured with $d = 34.5\,\mathrm{mm}$. The order of magnitude of the period T obtained with these diameters for $z_i/L \approx 0.5$ is $T \approx 0.25\,\mathrm{s}$. The evolution of the period is different for diameters smaller than 15 mm, since the period always increase from $z_i/L \approx 0$ to $z_i/L \approx 1$, with a kind of weak divergence close to $z_i/L \approx 1$.

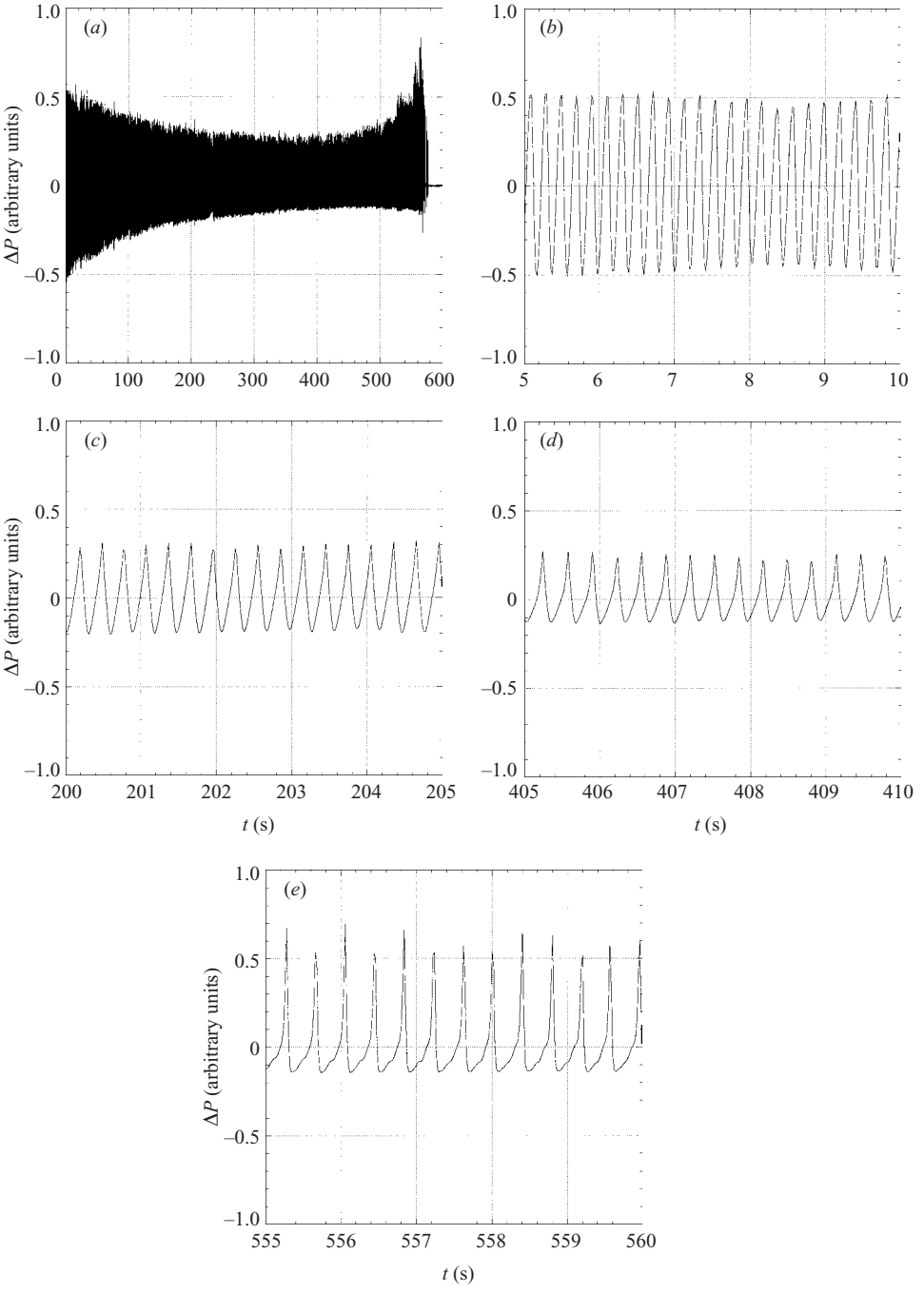

FIGURE 9. Pressure signal obtained with tube 2, water and $d = 10\,\text{mm}$: (*a*) whole recorded signal; (*b*) zoom in $t(\text{s}) \in [5, 10]$; (*c*) zoom in $t(\text{s}) \in [200, 205]$; (*d*) zoom in $t(\text{s}) \in [405, 410]$; (*e*) zoom in $t(\text{s}) \in [555, 560]$.

Tube 3 has the same diameter as tube 2 ($D_0 = 7.89\,\text{cm}$), but twice the length, $L = 1.75\,\text{m}$. The evolution of the period $T(z_i/L)$ measured in tube 3 with water is reported in figure 11(*a*). The period still increases when the diameter of the hole decreases. For diameters larger than 10 mm, the period is a weak function of the

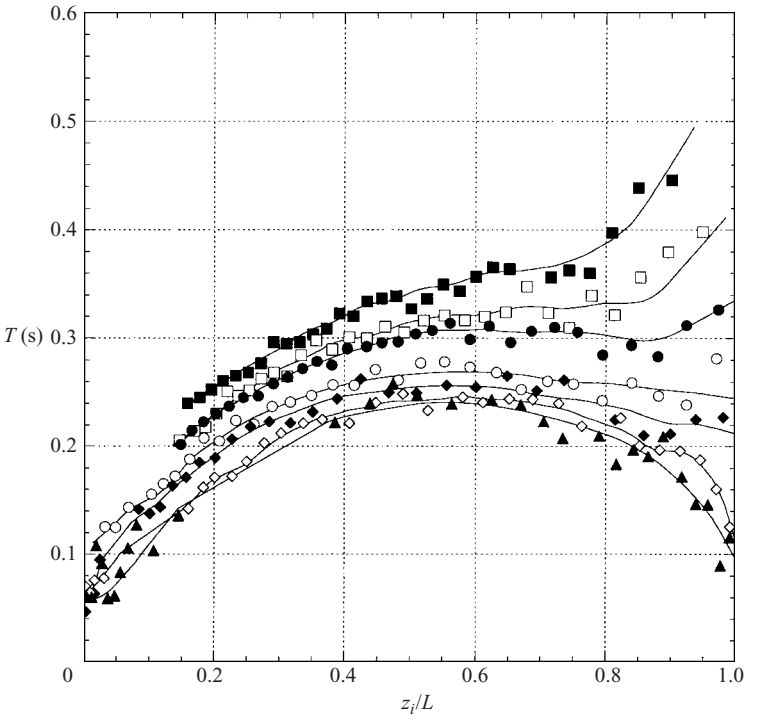

FIGURE 10. Evolution of the period T with the interface location z_i, in tube 2 with water for different diameter of holes: ■, $d = 9$ mm; □, 10 mm; ●, 12.4 mm; ○, 15.35 mm; ◆, 20 mm; ◇, 26.4 mm; ▲, 34.5 mm.

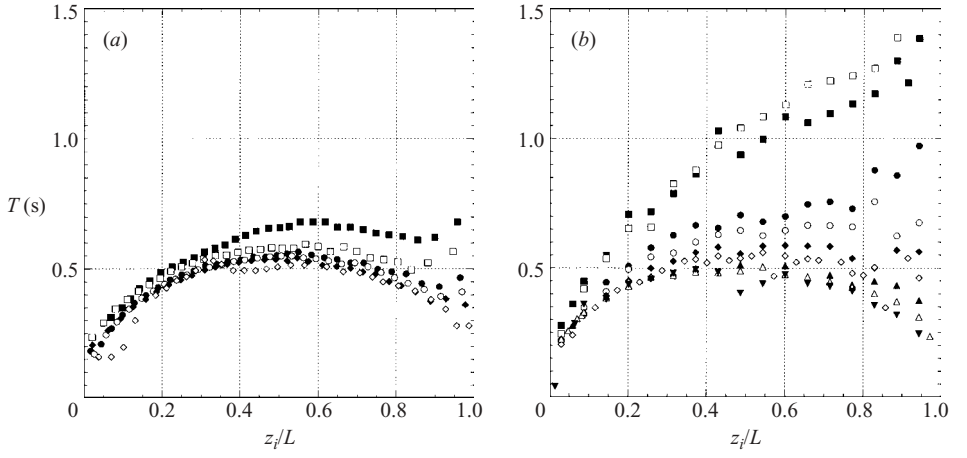

FIGURE 11. Evolution of the period T obtained with water in tube (*a*) 3 and (*b*) 1 using different hole diameters and presented as a function of the interface location z_i/L: (*a*) tube 3 with: ■, $d = 9$ mm; □, 10 mm; ●, 11.7 mm; ○, 13.5 mm; ◆, 15.35 mm; ◇, 34.5 mm; (*b*) tube 1 with: ■, $d = 10$ mm; □, 12.4 mm; ●, 15.35 mm; ○, 20 mm, ◆ $d = 26.4$ mm, ◇ $d = 34.5$ mm, ▲ $d = 45$ mm, △ $d = 59$ mm, ▼ $d = 77.4$ mm.

diameter and presents a maximum $T \approx 0.5$ s for $z_i/L \approx 0.5$. The maximum observed in similar conditions with tube 2 is $T \approx 0.25$ s. Doubling the length thus doubles the value of this maximum period.

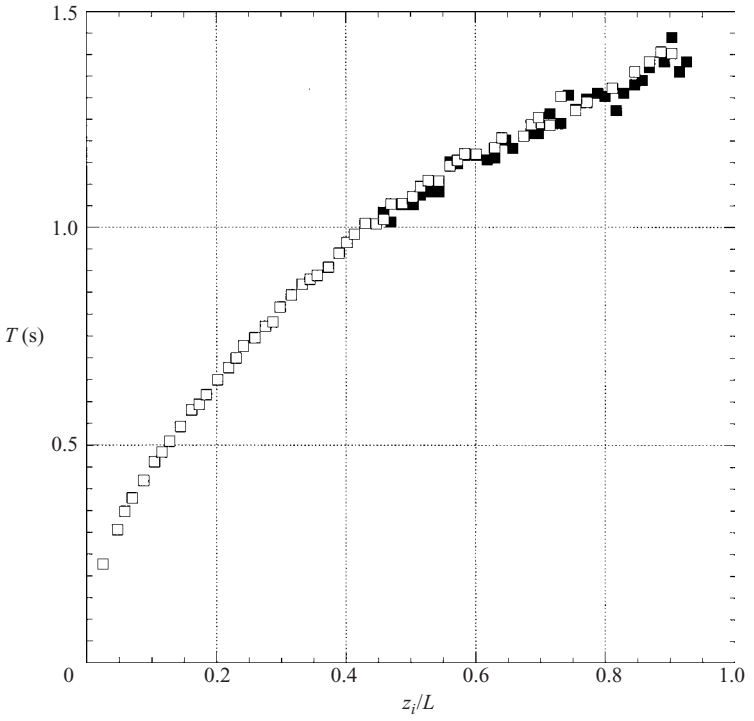

FIGURE 12. Evolution of the period of oscillation T obtained with water in tube 1 and $d = 12.4$ mm. The period is presented as a function of the relative interface location z_i/L, for two different initial conditions: ■, $z_i(t=0) = 80$ cm; □, $z_i(t=0) = 0$.

Tube 1 has the same length as tube 3 but twice the diameter $D_0 = 17.4$ cm. The evolution of the period measured with water in tube 1 is presented in figure 11(*b*) for different diameters. For diameters d larger than 34.5 mm, the period becomes a weak function of the diameter with a maximum $T \approx 0.5$ s obtained for $z_i/L \approx 0.5$. As the diameter is decreased, we observe a strong dependency of the period with the diameter: for $d = 10$ mm, the period is $T \approx 1$ s at the location $z_i/L \approx 0.5$. For diameters smaller than 20 mm, the period does not present any maximum and increases from $z_i/L = 0$ to $z_i/L = 1$.

The effect of the initial location of the interface $z_i(t=0)$ on the oscillations is presented in figure 12, where the trajectories obtained, in tube 1 and water ($d = 12.4$ mm), with $z_i(t=0) = 0$ cm and $z_i(t=0) = 80$ cm are reported. This figure shows that the initial condition has no influence on the period T.

The influence of the liquid viscosity on the period T is presented in figure 13(*a*). The measurements have been performed in tube 1 with water and the mixture of water and glycerol are presented in § 2. For the three different holes, the evolution of the period is similar for both liquids and we conclude that the period is not sensitive to the liquid viscosity as long as the Kapitsa number remains small. In figure 13(*b*) we report the evolution of the period with the interface location, observed in tube 2 using water and ethanol. We observe that the period obtained with ethanol is systematically smaller than the period obtained with the same hole with water. The difference for $z_i/L = 0.5$ is of the order of 15%. It will be seen later that this difference arises from the change in density and not from the change in surface tension.

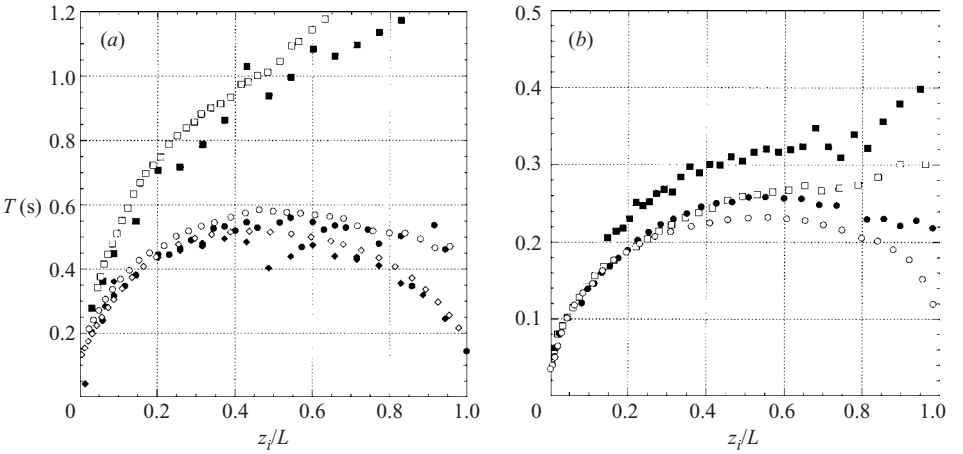

FIGURE 13. Effect of liquid properties. Evolution of the period T with the interface location: (a) tube 1 ■, $d = 10$ mm with water; □, 10 mm with water and glycerol; ●, 34.5 mm with water; ○, 34.5 mm with water and glycerol; ◆, 77 mm with water; ◇, 77 mm with water and glycerol; (b) tube 2 with: ■, $d = 10$ mm with water; □, 10 mm with ethanol; ●, 20.1 mm with water; ○, 20.1 mm with ethanol.

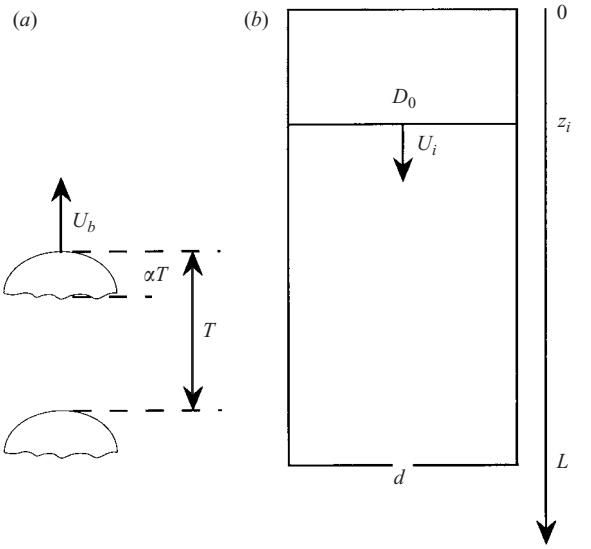

FIGURE 14. Model for the emptying time T_e: (a) on the short time scale T; (b) on the long time scale T_e.

4. Models

4.1. *On the long time scale T_e*

To model the dynamics of the liquid interface on the long time scale T_e, we assume that the long and short time scales are decoupled $T_e/T \gg 1$, so that on the long time scale, the emptying phenomenon appears as continuous. If α stands for the fraction of the period T during which air enters the bottle, the incoming volume of air is: $V_{air} = \alpha T U_b s$, where U_b is the characteristic rise velocity of the bubble and $s = \pi d^2/4$ the surface of the hole (figure 14a). On the long time scale, we can define V_{air}/T as

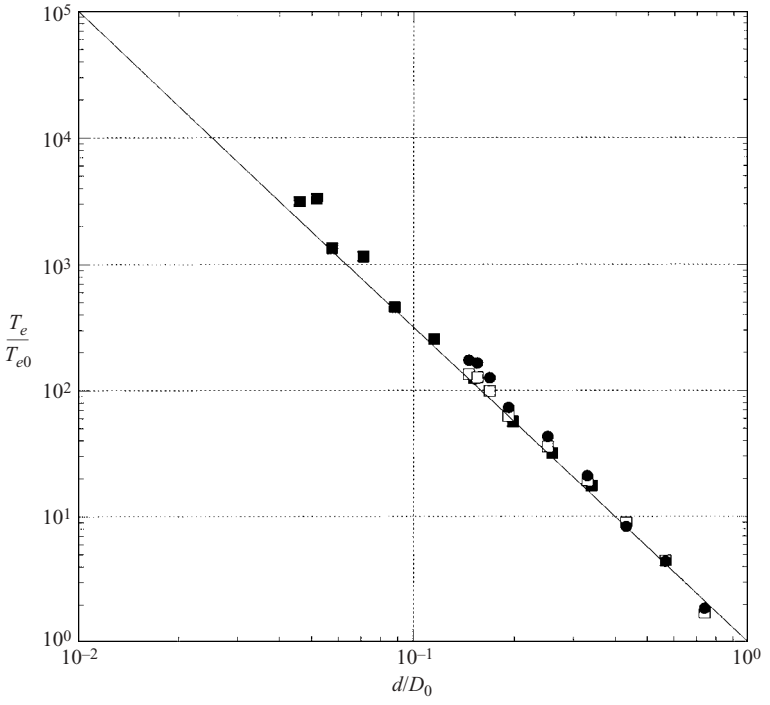

FIGURE 15. Comparison between the reduced emptying time T_e/T_{e0} and the model, equation (4.2) presented with a solid line: ■, tube 1; □, tube 2; ●, tube 3.

the volume of air that enters the tube by unit time. The constraint of constant volume then implies:

$$U_i D_0^2 = \alpha U_b d^2. \tag{4.1}$$

The velocity of bubbles larger than the capillary length and which rise in a low-viscosity liquid is known (Harper 1973) to scale as $U_b \propto \sqrt{g\mathscr{L}}$, where $\mathscr{L}$ is the characteristic length of the bubble. Davies & Taylor (1950) have shown that for a large single bubble rising in an infinite medium, $U_b \approx 2/3\sqrt{gR}$, where R is the radius of curvature at the apex. Here, we make the assumption that the characteristic length of the bubbles that enter the tube is d, the diameter of the hole, so that $U_b \propto \sqrt{gd}$. The emptying time of the tube $T_e = L/U_i$ can then be written:

$$\frac{T_e}{T_{e0}} = \left(\frac{D_0}{d}\right)^{5/2}, \tag{4.2}$$

where $T_{e0} \approx 3.0L/\sqrt{g.D_0}$ is the emptying time obtained with $d = D_0$ (Dumitrescu 1943; Davies & Taylor 1950). The comparison between the experimental measurements performed with water in the three different tubes is presented in figure 15.

The agreement is correct for a diameter range that extends over a decade. The emptying time can also be written as $T_e \propto D_0^2 L/(d^2\sqrt{(gd)})$. This time is independent of the liquid properties (ρ, ν, σ) and for a given diameter of hole d, it increases with the volume of the bottle $\propto D_0^2 L$. These tendencies are compatible with the observations reported in § 3.1.

Applying this model to the bottle presented in figure 1, we obtain $T_e \approx 10.4$ s, which is close to the observed value $T_e \approx 10$ s. The present model is also compatible with the observation of the linear decrease of the mass in time.

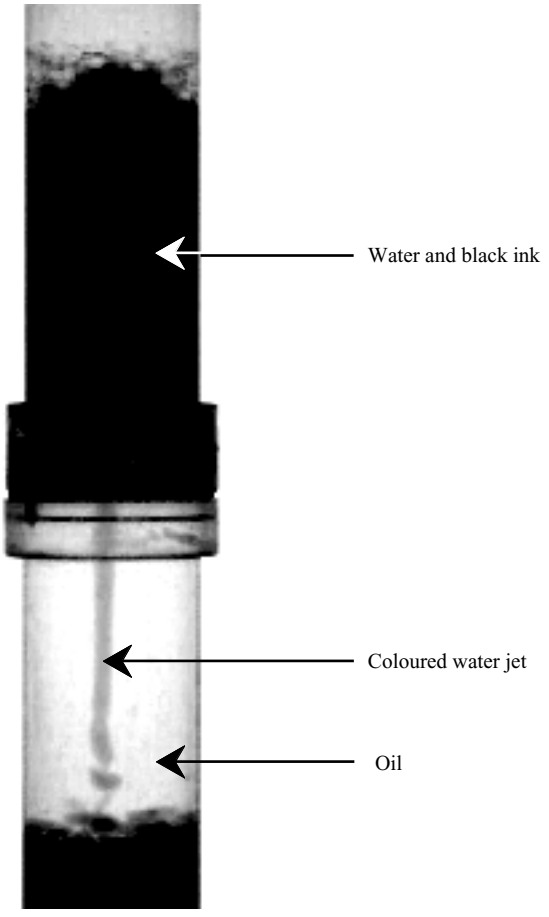

FIGURE 16. Experiment conducted with water and low-viscosity oil.

4.2. *On the short time scale T*

4.2.1. *Physical origin of the oscillations*

In figure 16, we present the experiment of a liquid sand-clock: it consists in two cylindrical tubes of equal diameter connected through a central thin-walled hole. The upper cylinder is initially filled with a liquid denser than the fluid in the lower part. At $t = 0$, the hole is opened and the flow starts. If the lower section is initially full of air, we observe an oscillatory regime, similar to the glug-glug observed in the tubes presented in § 3.2. In the experiment presented in figure 16, the upper cylinder is initially filled with coloured water and the lower one with a vegetable oil of low viscosity ($\nu \approx 15 \times 10^{-6}\,\mathrm{m^2\,s^{-1}}$). This oil is incompressible and not miscible with water. When the hole is opened, we observe a continuous exchange without oscillations, both liquids sharing the section of the hole.

This experiment shows that the physical origin of the oscillations of the glug-glug lies in the compressibility of the surrounding gas.

4.2.2. *Spring–mass analogy*

Prior to a more detailed model, we first propose a mechanical analogy for the glug-glug. We consider the syringe presented in figure 17(*a*), where a piston of section

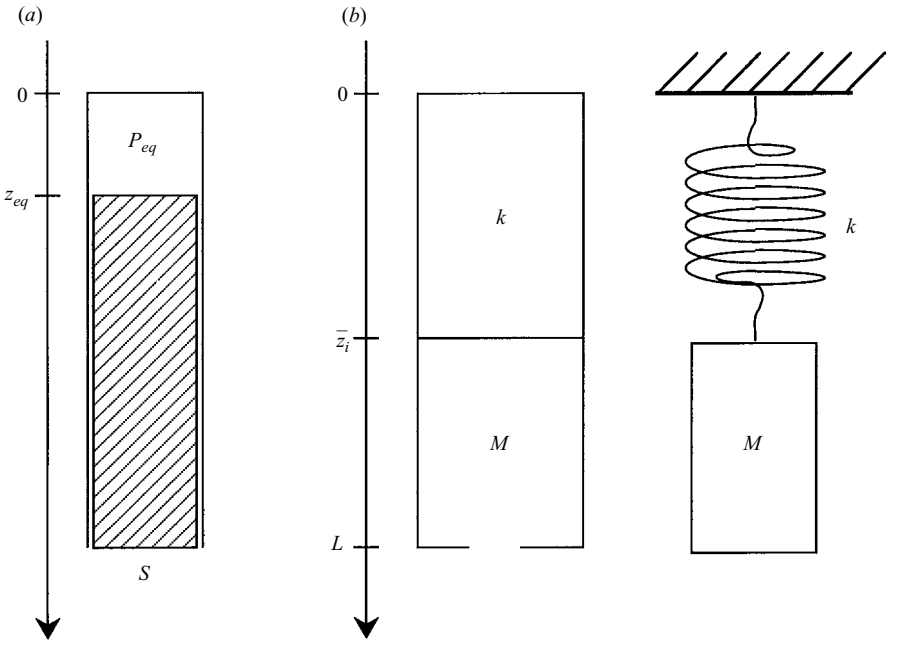

FIGURE 17. Mechanical analogy: (*a*) definition of a spring rigidity (*b*) mass–spring analogy.

S defines a volume of air $S z_{eq}$ with the pressure P_{eq}. As the piston is moved a distance δz from its equilibrium position z_{eq}, the pressure in the air changes by the amount δP such that: $\delta P/P_{eq} = -\gamma \delta z/z_{eq}$. We have assumed an isentropic transformation. The restoring force which acts on the piston $\delta F = \delta P\, S$ is thus proportional to the perturbation δz and we can define the rigidity $k \equiv \gamma P_{eq} S/z_{eq}$ such that $\delta F = -k\delta z$.

We now consider the glug-glug and propose the mass–spring analogy presented in figure 17(*b*). According to the syringe argument, $k \equiv \gamma P_0 S/\bar{z}_i$. The mass of water is $M = \rho S\,(L - \bar{z}_i)$ and the period $T = 2\pi\sqrt{M/k}$ takes the form:

$$T = 2\pi \frac{L}{\sqrt{\gamma P_0/\rho}} \sqrt{\frac{\bar{z}_i}{L}\left(1 - \frac{\bar{z}_i}{L}\right)}. \tag{4.3}$$

The dimension of T results from the ratio of the length L to the speed $\sqrt{P_0/\rho}$. This speed is a combination of the compressibility of the gas and the inertia of the liquid. In this sense, it resembles the speed of sound in bubbly liquids (van Wijngaarden 1982).

More quantitatively, the linearity between T and L at a given $\bar{z}_i/L$, predicted by (4.3), is compatible with the observations reported in § 3.2. The period depends on the fluid properties through $\sqrt{\rho}$ and not through the viscosity or surface tension (§ 3.2). Moreover, the behaviour in $\bar{z}_i\,(1 - \bar{z}_i)$ which leads to $T = 0$ at $z_i = 0$ and $z_i = L$ with a maximum at $z_i = L/2$ is also compatible with the measurements performed with holes of large diameter. Quantitatively, for $L = 1.7$ m and $z_i = L/2$, we calculate $T \approx 0.45$ s, which is consistant with the observed value $T \approx 0.5$ s, obtained again with the large values of d/D_0. Despite these positive tendencies, the above linear model does not capture the influence of the diameter of the hole on the period of the oscillations, presented in figure 11.

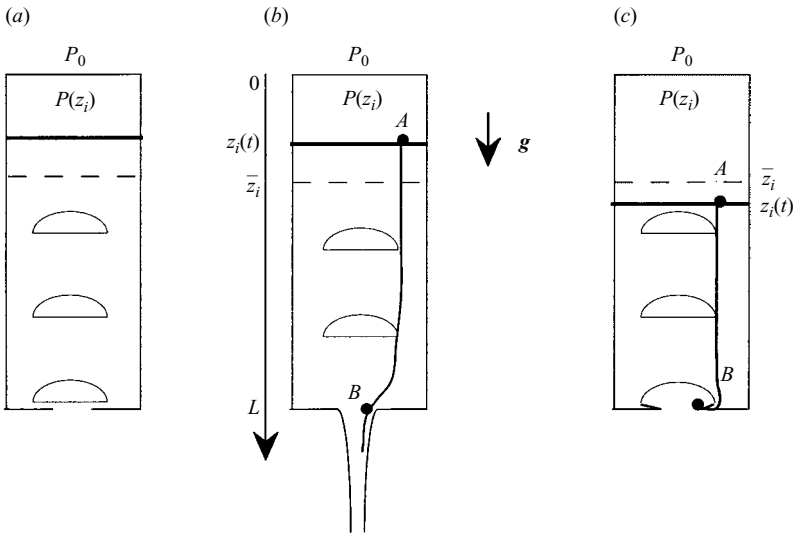

FIGURE 18. Model for the oscillations.

4.2.3. *A more detailed model*

A more detailed model for the oscillations is presented in figure 18: the cycle starts at the entrance of a bubble in the tube (figure 18*a*). The oscillation is then decomposed into two phases: an outflow of the liquid (figure 18*b*) and the admission of a new bubble without liquid flow (figure 18*c*). Since the emptying time T_e is large compared to the period T, we assume that, during the whole period, the mean position of the interface $\bar{z}_i$ is constant. The actual interface location z_i is thus decomposed into a fixed part $\bar{z}_i$ and a time-dependent part $\tilde{z}_i$: $z_i(t) = \bar{z}_i + \tilde{z}_i(t)$. We expect this model to be valid as soon as the upper volume of air is larger than the volume of bubbles contained in the tube†. To describe the motion of the liquid in the tube during the whole cycle, we use Euler's equation:

$$\frac{\partial \boldsymbol{U}}{\partial t} + \nabla \boldsymbol{U} \cdot \boldsymbol{U} = -\frac{1}{\rho}\nabla p + \boldsymbol{g}. \tag{4.4}$$

Projecting (4.4) onto a streamline and integrating between the points A and B, respectively located on the upper interface and the exit of the tube (see figure 18), we obtain:

$$\int_A^B \frac{\partial \boldsymbol{U}}{\partial t} \cdot \mathrm{d}l + \tfrac{1}{2}\left(U_B^2 - U_A^2\right) = -\frac{1}{\rho}(P_B - P_A) + g(L - z_i). \tag{4.5}$$

In this equation, $\mathrm{d}l$ represents an element of the streamline. During the cycle, the mass of air remains almost constant in the upper part of the tube. Since the period of oscillation (of the order of the second) is short compared to the time of thermal equilibrium, D_0^2/D_{th}, where D_{th} is the thermal diffusivity of air, we assume an isentropic transformation and deduce:

$$P_A V_A^{\gamma} = P_{eq} V_{eq}^{\gamma}, \tag{4.6}$$

† This condition is satisfied when $z_i > (d/D_0)^2 L$. Since $z_i = U_i t$, we conclude that the model starts to be valid when $t > L/\sqrt{gd}$. In the limit $d < D_0$ where the glug-glug is studied, this time is much smaller than the emptying time T_e and this condition only affects the first periods of oscillation.

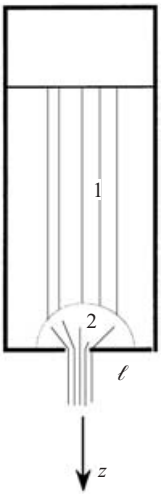

FIGURE 19. Model of the outflow.

where P_A and V_A represent the pressure and the volume of the air when the interface is at z_i. P_{eq} and V_{eq} have the same meaning but for the equilibrium location and can be expressed as functions of $\bar{z}_i$:

$$V_{eq} = \tfrac{1}{4}\pi D_0^2 \bar{z}_i, \tag{4.7}$$

$$P_{eq} = P_0 \left[1 - \lambda\left(1 - \frac{\bar{z}_i}{L}\right)\right]. \tag{4.8}$$

In (4.8), $\lambda \equiv \rho g L/P_0$ measures the maximal equilibrium depression of the air. In our experiments, λ is a small constant, equal to 0.17 in tubes 1 and 3 and equal to 0.08 in tube 2. From (4.6), we deduce the expression of the pressure at A. The pressure at B is equal to P_0. The right-hand side of (4.5) can be linearized to yield:

$$-\frac{1}{\rho}(P_B - P_A) + g(L - z_i) = -\frac{\gamma P_0}{\rho \bar{z}_i}\tilde{z}_i F(\lambda, \bar{z}_i), \tag{4.9}$$

where $F(\lambda, \bar{z}_i) \equiv [1 - \lambda + \lambda(\bar{z}_i/L)(1 + 1/\gamma)]$. In our study, λ is small compared to unity and $F(\lambda, \bar{z}_i) \approx 1$. We now concentrate on the left-hand side of (4.5), considering first the outflow.

During the outflow (figure 18), the velocity at B is higher than the velocity at A by the ratio $(D_0/d)^2$. We deduce:

$$\tfrac{1}{2}\left(U_B^2 - U_A^2\right) = \frac{1}{2}\left[\left(\frac{D_0}{d}\right)^4 - 1\right]\dot{\tilde{z}}_i^2. \tag{4.10}$$

To evaluate the acceleration term $\int_A^B \partial \boldsymbol{U}/\partial t \cdot \mathrm{d}l$, we assume that the flow has the structure presented in figure 19: the flow is decomposed into two regions, a uniform region which extends from the interface to a location close to the hole (region 1) and the second which is close to the hole. In region 1, the flow is approximated by $\boldsymbol{U} \approx \dot{\tilde{z}}_i \boldsymbol{e}_z$. In region 2, we assume a radial sink flow of the type $v_r = \alpha (D_0/r)^2 \dot{\tilde{z}}_i$, where α is a constant. Using mass conservation we find that region 2 extends from $r = \sqrt{\alpha} d$ (where $v_r = (D_0/d)^2 \dot{\tilde{z}}_i$) to $r = \ell = \sqrt{\alpha} D_0$ (where $v_r = \dot{\tilde{z}}_i$). This structure of the flow

leads to:

$$\int_A^B \boldsymbol{U}\cdot \mathrm{d}l \approx (L-\sqrt{\alpha}D_0 - z_i)\dot{\bar{z}}_i + \int_{\sqrt{\alpha}d}^{\sqrt{\alpha}D_0} \alpha\left(\frac{D_0}{r}\right)^2 \dot{\bar{z}}_i \mathrm{d}r, \tag{4.11}$$

from which we deduce the acceleration term:

$$\int_A^B \frac{\partial \boldsymbol{U}}{\partial t}\cdot \mathrm{d}l \approx \left[L-\bar{z}_i + \sqrt{\alpha}\frac{D_0^2}{d}\left(1-2\frac{d}{D_0}\right)\right]\ddot{\bar{z}}_i = (L-\bar{z}_i+\mathscr{L})\ddot{\bar{z}}_i, \tag{4.12}$$

where the length $\mathscr{L}\equiv\sqrt{\alpha}D_0^2/d\,(1-2d/D_0)$ accounts for the liquid acceleration at the hole. The Euler equation, (4.5), during the outflow can thus be written:

$$(L-\bar{z}_i+\mathscr{L})\ddot{\bar{z}}_i + \frac{1}{2}\left[\left(\frac{D_0}{d}\right)^4 - 1\right]\dot{\bar{z}}_i^2 + \frac{\gamma P_0}{\rho \bar{z}_i}\tilde{z}_i F(\lambda, \bar{z}_i) = 0. \tag{4.13}$$

During the entry of the bubble into the tube (figure 18*b*), we proceed through the same stages, but with the new condition $U_B = 0$. The strong nonlinear term disappears in this case and the dynamics of the interface is described by the equation:

$$\ddot{\bar{z}}_i(L-\bar{z}_i) - \tfrac{1}{2}\dot{\bar{z}}_i^2 + \frac{\gamma P_0}{\rho \bar{z}_i}\tilde{z}_i F(\lambda, \bar{z}_i) = 0. \tag{4.14}$$

Since we look for small oscillations around the equilibrium, in both equations we retain only the linear terms. The dynamics of the interface during the whole cycle is thus described by the system:

$$\ddot{\tilde{z}}_i + \frac{\gamma P_0}{\rho L^2}\frac{F(\lambda, \bar{z}_i)}{\bar{z}_i/L}\frac{1}{1-\bar{z}_i/L+\mathscr{L}/L}\tilde{z}_i = 0, \tag{4.15}$$

$$\ddot{\tilde{z}}_i + \frac{\gamma P_0}{\rho L^2}\frac{F(\lambda, \bar{z}_i)}{\bar{z}_i/L}\frac{1}{1-\bar{z}_i/L}\tilde{z}_i = 0, \tag{4.16}$$

the first equation describing $\dot{\bar{z}}_i > 0$ and the second $\dot{\bar{z}}_i < 0$. This linearization of the problem enables us to find an analytical expression for the period of the oscillations:

$$T = \pi\frac{L}{\sqrt{\gamma P_0/\rho}}\sqrt{\frac{\bar{z}_i/L}{F(\lambda, \bar{z}_i)}}\left[\sqrt{1-\bar{z}_i/L} + \sqrt{1-\bar{z}_i/L+\sqrt{\alpha}\frac{D_0^2}{dL}\left(1-2\frac{d}{D_0}\right)}\right]. \tag{4.17}$$

In the limit $\lambda \ll 1$ and $D_0^2/(dL) \ll 1$, we recover the period given by the spring–mass analogy (4.3). To evaluate the value of the free parameter α, we have adjusted its value in one set of experiments (obtained with tube 1). Using $\alpha = 4.8$, the comparison between the period measured experimentally and the period calculated with (4.17) is presented in figure 20 for the three different tubes, and a range of exit diameters.

The comparison conducted in tube 1 (figure 20*a*) first shows that the spring–mass approximation of the period (4.3) is satisfactory for hole diameters larger than 45 mm. For smaller diameters, the period increases and the linearized detailed model (4.17) captures the overall influence of the diameter. The main discrepancies occur when the interface becomes close to the hole.

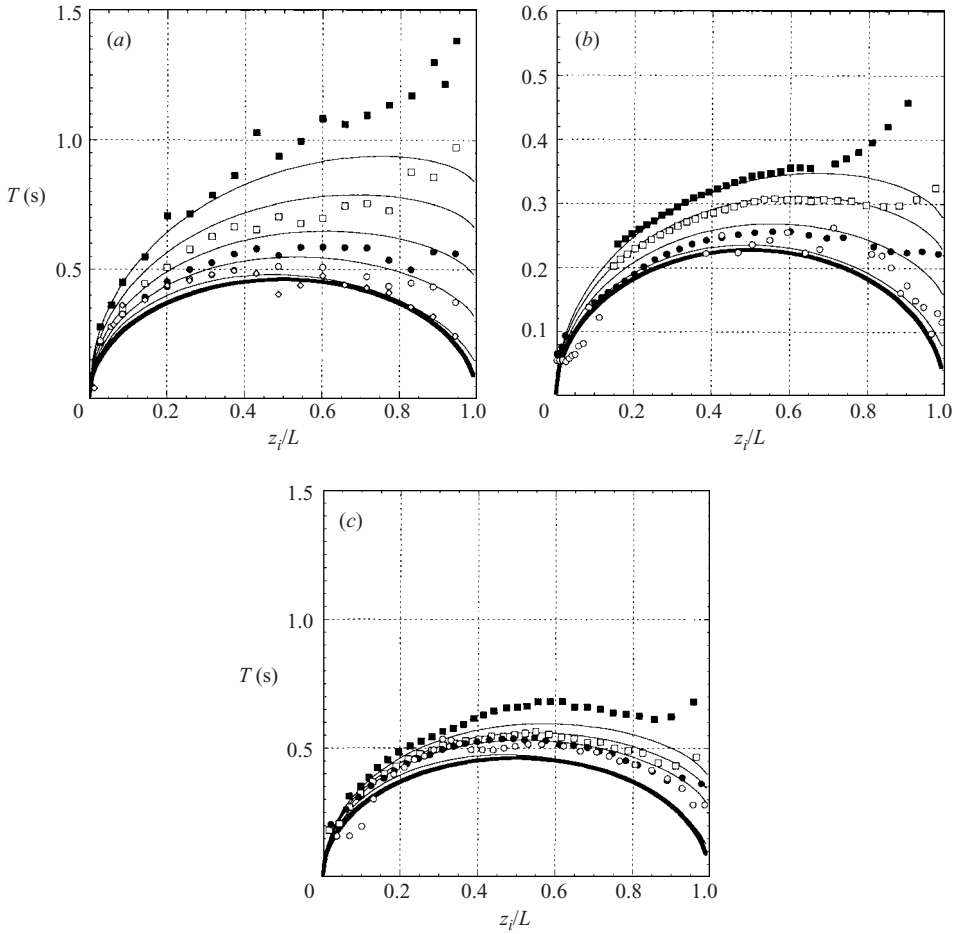

FIGURE 20. Comparison between the period T measured experimentally and the period calculated from (4.17) with $\alpha = 4.8$: (*a*) tube 1: ■, $d = 10$ mm; □, 15.35 mm; ●, 26.4 mm; ○, 45.2 mm; ◇, 77.5 mm; (*b*) tube 2: ■, $d = 9$ mm; □, 12.4 mm; ●, 20.1 mm; ○, 34.5 mm; (*c*) tube 3: ■, $d = 9$ mm; □, 11.7 mm; ●, 15.35 mm; ○, 34.5 mm; the thin lines are the periods calculated with (4.17) and the bold line is (4.3).

The same comments can be made for the comparison conducted in tubes 2 and 3 and presented, respectively, in figures 20(*b*) and 20(*c*). The spring–mass approximation captures the evolution of the period for the larger diameters and the linearized detailed model is reasonably able to follow its evolution for smaller diameters. Again, the main descrepencies are observed when the interface aproaches the hole.

From experiment, we have noticed in § 3.2, that the difference in the period between the different diameters increases when D_0/d increases and when the interface is close to $z_i = L$. At the same time, the pressure oscillations in the tube become non-sinusoidal (see figure 9). From (4.13), both behaviours can be understood as an effect of the nonlinear term $\propto (D_0/d)^4 \tilde{z}_i^2$ that has been neglected in our linearized analysis. Better agreement with the experimental results can be obtained through numerical integration of (4.13) and (4.14).

Applying this model to the bottle presented in figure 1, we obtain the evaluation $T \approx 0.065$ s. We have used the following values in the calculation $\bar{z}_i/L = 0.5$,

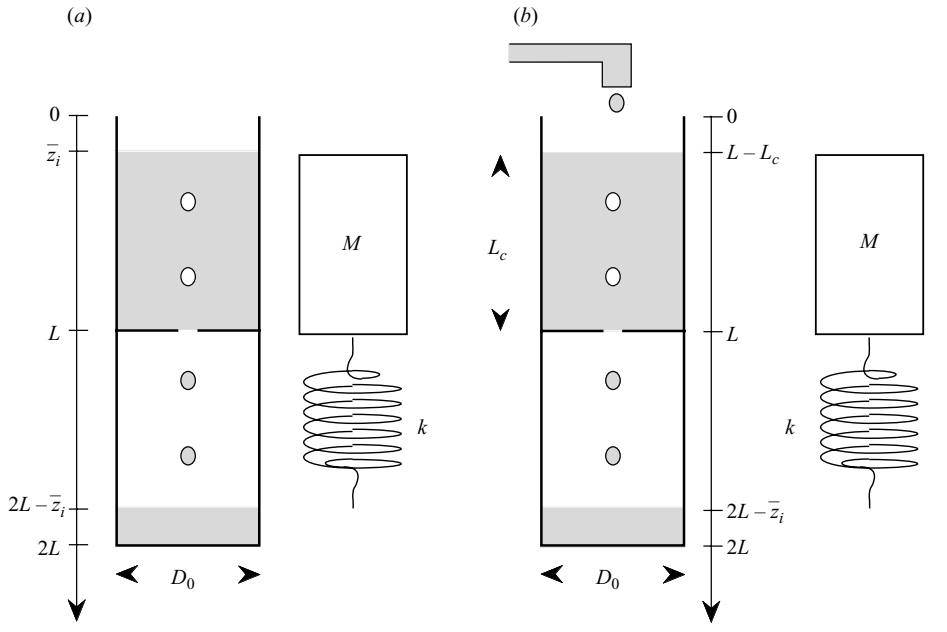

FIGURE 21. Presentation of two different glug-glugs: (*a*) tube 4, (*b*) tube 5.

$L = 0.23\,\mathrm{m}$, $D = 0.065\,\mathrm{m}$, $d = 0.024\,\mathrm{m}$, $P_0 = 10^5\,\mathrm{Pa}$ and $\rho = 820\,\mathrm{kg\,m^{-3}}$. This value of the period of oscillation is compatible with the measured period, $T \approx 0.07$.

5. Two other glug-glugs

The analysis developed for the long and short time scales of the emptying of the bottle are applied in this section to the configurations presented in figure 21. In tube 4 (figure 21*a*), two cylinders of diameter $D_0 = 8\,\mathrm{cm}$ and length $L = 0.86\,\mathrm{m}$ are coupled via a central thin-walled hole of diameter d. The upper cylinder is open at the top and initially full of liquid. The lower cylinder is closed at the bottom and initially full of air. At $t = 0$, the hole is open and the glug-glug starts. At the end of the process, the lower tube is full and the upper one is empty. Tube 5 (figure 21*b*) is identical to tube 4 except that the liquid level in the upper part is kept constant and equal to $L_c = 68\,\mathrm{cm}$. At the end of the process, the lower tube is full and the upper one always contains water up to L_c.

Considering the long time scale T_e, figure 22 presents the evolution of the emptying time in tubes 2, 4 and 5. In the case of tube 5, T_e is the time needed to fill the lower tube. We observe in figure 22, that for a given diameter of hole, the emptying time is identical in the three experiments. Since L and D_0 are the same for tubes 2, 4 and 5, this result is expected from the analysis presented in § 4.1.

The evolution of the short time scale T in tube 4 and 5 is presented in figure 23. For tube 4 (figure 23*a*), the period decreases almost linearly from 0.5 s down to 0.1 s as the mean position of the interface moves from $\bar{z}_i = 0$ to $\bar{z}_i = L$. We observe a small influence of the diameter of the hole: the period increases slightly when the diameter decreases. If we apply spring–mass analogy to this configuration, we find the rigidity $k \equiv \gamma P_0 S/(L - \bar{z}_i)$ and the mass $M \equiv \rho S(L - \bar{z}_i)$. We deduce the evolution of the

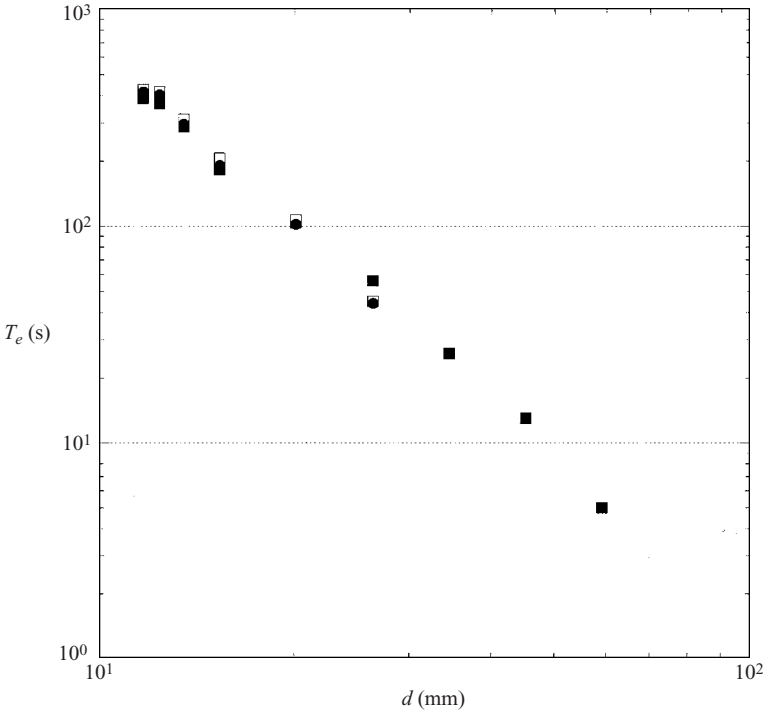

FIGURE 22. Evolution of the long time scale T_e in the different tubes: ■, tube 2; □, tube 4; ●, tube 5.

period $T \equiv 2\pi\sqrt{M/k}$:

$$T = 2\pi \frac{L}{\sqrt{\gamma P_0/\rho}} \left(1 - \frac{\bar{z}_i}{L}\right). \tag{5.1}$$

This simple evaluation of the period is represented by the solid line in figure 23(*a*). The order of magnitude of the period is correct, as well as the linear evolution with the interface location. However, we see that the difference between this linear evaluation and the measurements increases as the mass of the liquid decreases. It is necessary to include both the effect of the acceleration of the liquid due to the hole and the effect of the nonlinear terms to correct the simple evaluation of the period given by (5.1).

In tube 5, the period T is also a decreasing function of the interface location and is presented in figure 23*b*. This decrease is not linear. If we apply the spring–mass analogy to this configuration, we find the rigidity $k \equiv \gamma P_0 S/(L - \bar{z}_i)$ and the mass $M \equiv \rho S L_c$. The period $T \equiv 2\pi\sqrt{M/k}$ is then:

$$T = 2\pi \frac{L}{\sqrt{\gamma P_0/\rho}} \sqrt{\frac{L_c}{L}} \sqrt{1 - \frac{\bar{z}_i}{L}}. \tag{5.2}$$

This linear evaluation is represented by the solid line in figure 23(*b*). The order of magnitude and the tendency are again consistent with the measurements.

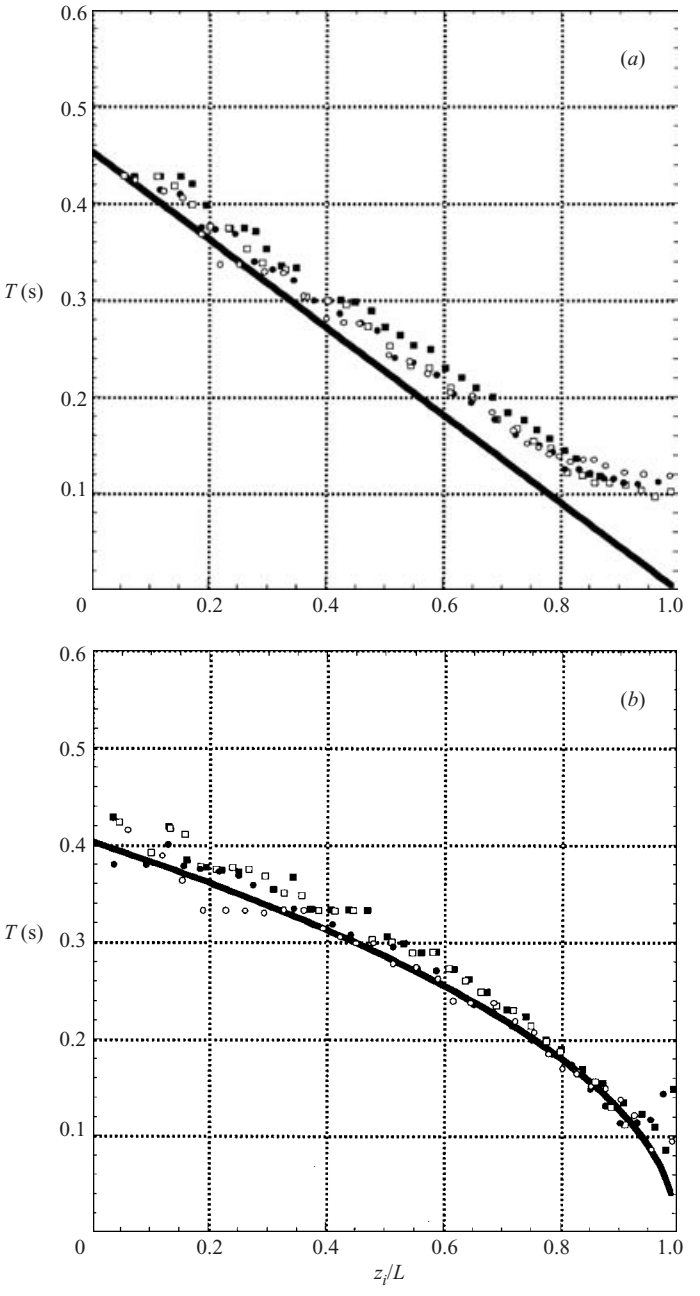

FIGURE 23. Evolution of the short time scale T in the different tubes: (*a*) tube n°4: ■ $d = 12.4$ mm, □ $d = 13.5$ mm, ● $d = 15.35$ mm, ○ $d = 20.1$ mm, the solid bold line represent the period derived from the spring-mass analogy (5.1); (*b*) tube n°5: ■ $d = 11.7$ mm, □ $d = 12.4$ mm, ● $d = 13.5$ mm, ○ $d = 20.1$ mm. the solid bold line represent the period derived from the spring-mass analogy (5.2).

6. Conclusion

We report the study of the glug-glug of the bottle, idealized as a vertical cylinder of diameter D_0, length L and open through a thin-walled hole of diameter d. We show

that the phenomenon is characterized by two distinct time scales: the long time scale of emptying T_e and the short time scale of the oscillation T.

On the long time scale, the phenomenon is continuous and the characteristic time can be evaluated by an extension of the propagation time of long bubbles. We show that:

$$T_e \sim \frac{L}{\sqrt{gD_0}} \left(\frac{D_0}{d}\right)^{5/2}.$$

On the short time scale, the interface oscillates around a mean position $\bar{z}_i$. We first show that the physical origin of the oscillations lies in the compressibility of the surrounding gas. In a second stage, we demonstrate that the oscillations can be modelled to first order by a spring–mass analogy and find:

$$T = \frac{L}{\sqrt{\gamma P_0/\rho}} \Phi(\bar{z}_i/L).$$

The function $\Phi(\bar{z}_i/L)$ depends on the configuration. This linear approximation holds provided the diameter of the hole is not too small and provided the mass of liquid which oscillates does not vanish. In these latter cases, the acceleration of the liquid at the hole must be accounted for as well as nonlinear terms that arise in the oscillations.

We wish to thank the students Pierre Héraud, Géraldine Abrami from the École Supérieur de Physique de Strasbourg and Lionel Castillon from the École Polytechnique who all helped to provide some of the experimental data. We also thank William Gilbert from the École Polytechnique who provided the data for the real bottle. We thank Emmanuel Villermaux with whom the discussion started around the tic-tac paper of D. Bideau. Finally, we thank J. Hinch for his interest in the subject and for his comments which have improved the final version of the manuscript.

REFERENCES

Le Pennec, T., Maloy, K. J., Hansen, A., Ammi, M., Bideau, D. & Wu, X. I. 1994 Ticking hour glasses : experimental analysis of intermittent flow. *Phys. Rev.* E **53**, 2257–2264.

Bideau, D., Madani, A. & Hansen, A. 1994 Le tic-tac du sablier. *La Recherche* **261**, 92–93.

Calder, W. A 1984 *Size, Function, and Life History*. Dover.

Clanet, C. 2000 From Galilei to Torricelli. *Phys. Fluids* **12**, 2743–2751.

Davies, R. M. & Taylor, G. I. 1950 The mechanics of large bubbles rising through extended liquids and through liquids in tubes. *Proc. R. Soc. Lond.* A **200**, 375–390.

Dumitrescu, D. T. 1943 Strömung an einer Luftblase im senkrechten Rohr. *Z. angew. Math. Mech.* **23**, 139–149.

Dukler, A. E. & Fabre, J. 1994 Gas–liquid slug flow knots and loose ends. In *Multiphase Science and Technology. Two Phase Flow Fundamentals* (ed. G. F. Hewitt *et al.*), vol, 8, pp. 355–470. Begell House.

Fabre, J. & Line, A. 1992 Modelling of two phase slug flow. *Annu. Rev. Fluid Mech.* **24**, pp. 21–46.

Harper, J. F. 1973 The motion of bubbles and drops through liquids. *Adv. Appl. Mech.* **12**, 59–129.

Prandtl, L. 1952 *Guide à travers la Mécanique des Fluides*. Albert Monod Dunod, Paris.

van Wijngaarden, L. 1952 *Mechanics and Physics of Bubbles in Liquids*. Kluwer.

Zukoski, E. E. 1966 Influence of viscosity, surface tension, and inclination angle on motion of long bubbles in closed tubes. *J. Fluid Mech.* **25**, 821–837.